

# Deflagrations in hybrid CONe white dwarfs: a route to explain the faint Type Iax supernova 2008ha

M. Kromer,<sup>1\*</sup> S. T. Ohlmann,<sup>2,3</sup> R. Pakmor,<sup>3</sup> A. J. Ruiter,<sup>4,5</sup> W. Hillebrandt,<sup>6</sup>  
K. S. Marquardt,<sup>2,3</sup> F. K. Röpkke,<sup>3,7</sup> I. R. Seitenzahl,<sup>4,5</sup> S. A. Sim<sup>5,8</sup> and S. Taubenberger<sup>6,9</sup>

<sup>1</sup>The Oskar Klein Centre & Department of Astronomy, Stockholm University, AlbaNova, SE-106 91 Stockholm, Sweden

<sup>2</sup>Institut für Theoretische Physik und Astrophysik, Universität Würzburg, Emil-Fischer-Straße 31, D-97074 Würzburg, Germany

<sup>3</sup>Heidelberger Institut für Theoretische Studien, Schloss-Wolfsbrunnengasse 35, D-69118 Heidelberg, Germany

<sup>4</sup>Research School of Astronomy & Astrophysics, Mount Stromlo Observatory, Cotter Road, Weston ACT 2611, Australia

<sup>5</sup>ARC Centre of Excellence for All-Sky Astrophysics (CAASTRO)

<sup>6</sup>Max-Planck-Institut für Astrophysik, Karl-Schwarzschild-Str. 1, D-85748 Garching bei München, Germany

<sup>7</sup>Zentrum für Astronomie der Universität Heidelberg, Institut für Theoretische Astrophysik, Philosophenweg 12, D-69120 Heidelberg, Germany

<sup>8</sup>Astrophysics Research Centre, School of Mathematics and Physics, Queen's University Belfast, Belfast BT7 1NN, UK

<sup>9</sup>European Southern Observatory, Karl-Schwarzschild-Str. 2, D-85748 Garching bei München, Germany

Accepted, 17 April 2015. Received, 14 March 2015; in original form, 14 March 2015

## ABSTRACT

Stellar evolution models predict the existence of hybrid white dwarfs (WDs) with a carbon–oxygen core surrounded by an oxygen–neon mantle. Being born with masses  $\sim 1.1 M_{\odot}$ , hybrid WDs in a binary system may easily approach the Chandrasekhar mass ( $M_{\text{Ch}}$ ) by accretion and give rise to a thermonuclear explosion. Here, we investigate an off-centre deflagration in a near- $M_{\text{Ch}}$  hybrid WD under the assumption that nuclear burning only occurs in carbon-rich material. Performing hydrodynamics simulations of the explosion and detailed nucleosynthesis post-processing calculations, we find that only  $0.014 M_{\odot}$  of material is ejected while the remainder of the mass stays bound. The ejecta consist predominantly of iron-group elements, O, C, Si and S. We also calculate synthetic observables for our model and find reasonable agreement with the faint Type Iax SN 2008ha. This shows for the first time that deflagrations in near- $M_{\text{Ch}}$  WDs can in principle explain the observed diversity of Type Iax supernovae. Leaving behind a near- $M_{\text{Ch}}$  bound remnant opens the possibility for recurrent explosions or a subsequent accretion-induced collapse in faint Type Iax SNe, if further accretion episodes occur. From binary population synthesis calculations, we find the rate of hybrid WDs approaching  $M_{\text{Ch}}$  to be on the order of 1 percent of the Galactic SN Ia rate.

**Key words:** supernovae: individual: SN 2008ha – methods: numerical – hydrodynamics – radiative transfer – nuclear reactions, nucleosynthesis, abundances – stars:evolution

## 1 INTRODUCTION

Type Iax supernovae (SNe Iax) form a distinct class of astronomical transients (Foley et al. 2013) with SN 2002cx (Li et al. 2003; Branch et al. 2004; Jha et al. 2006) as the proto-typical example. It has been argued that SNe Iax occur at a rate of 5 to 30 percent of the overall rate of Type Ia supernovae (SNe Ia) (Li et al. 2011b; Foley et al. 2013; White et al. 2015). Recently, McCully et al. (2014) reported the first detection of a progenitor candidate for a SN Iax. In pre-explosion *Hubble Space Telescope* (*HST*) images they discovered a point source at the location of SN 2012Z. Future *HST* observations will show whether this point source is actually a massive star that exploded giving rise to the SN, or a He donor to an accret-

ing carbon–oxygen (CO) white dwarf (WD) as argued by McCully et al. (2014).

Although spectroscopically similar to SNe Ia, SNe Iax are characterized by distinctive features: (i) expansion velocities at maximum light (2000 to  $8000 \text{ km s}^{-1}$ ) that are significantly lower than those of SNe Ia (10,000 to  $15,000 \text{ km s}^{-1}$ , e.g. Foley et al. 2013; Stritzinger et al. 2015), (ii) low peak absolute magnitudes with respect to the width–luminosity relation of SN Ia light curves (e.g. McClelland et al. 2010; Stritzinger et al. 2014), (iii) peculiar late-time spectra that differ strongly from other SNe (e.g. Jha et al. 2006; Sahu et al. 2008) and (iv) a statistical association with star-formation regions (so far no SN Iax has been observed in elliptical galaxies), indicating short delay times of 30 to 50 Myr (Lyman et al. 2013).

SNe Iax show significant diversity in peak absolute magni-

\* E-mail: markus.kromer@astro.su.se

tude and expansion velocities. For example, SN 2005hk, one of the brighter class members, peaked at  $M_{\text{max}}^V \sim -18.1$  mag (Chornock et al. 2006; Phillips et al. 2007; Sahu et al. 2008). In contrast, SN 2008ha, to date the faintest member of the class, reached only  $M_{\text{max}}^V \sim -14.2$  mag (Foley et al. 2009; Valenti et al. 2009; Foley et al. 2010). This indicates a wide range of ejecta properties.

Several explosion mechanisms have been proposed for SNe Iax, including core collapse of massive stars (Foley et al. 2009; Valenti et al. 2009; Moriya et al. 2010), detonations in He shells on top of CO WDs (Foley et al. 2009) and deflagrations or pulsational delayed detonations in near Chandrasekhar-mass ( $M_{\text{Ch}}$ ) CO WDs (Branch et al. 2004; Phillips et al. 2007; Stritzinger et al. 2015). The mechanism that seems to agree best with the observed properties of SNe Iax, including the possible detection of a stellar remnant for the faint Type Iax SN 2008ha (Foley et al. 2014b), is a deflagration in a near- $M_{\text{Ch}}$  CO WD that fails to completely unbind the WD, leaving behind a bound remnant (Foley et al. 2009).

Jordan et al. (2012) were the first to present hydrodynamical simulations of this scenario yielding  $^{56}\text{Ni}$  and total ejecta masses in agreement with the observationally derived quantities for bright SNe Iax. Combining detailed explosion models and radiative transfer simulations, Kromer et al. (2013) have shown that pure deflagrations in near- $M_{\text{Ch}}$  CO WDs that leave behind a compact remnant can indeed reproduce the observational display of the brighter SNe Iax like SNe 2002cx or 2005hk. Fink et al. (2014) have confirmed these results with a set of models exploring deflagrations in near- $M_{\text{Ch}}$  CO WDs for different ignition setups. However, they fail to explain the faint class members like SN 2008ha (their faintest model yields  $M_{\text{max}}^V = -16.8$  mag while SN 2008ha peaks at  $-14.2$  mag; Foley et al. 2009). Although Jordan et al. (2012) and Fink et al. (2014) did not fully explore the parameter space of possible ignition configurations, it seems implausible to reach low enough  $^{56}\text{Ni}$  masses to explain the low luminosities of the faintest SNe Iax from deflagrations in near- $M_{\text{Ch}}$  CO WDs.

To explain these events with deflagrations in near- $M_{\text{Ch}}$  WDs, one somehow has to quench burning at an early stage to reduce the  $^{56}\text{Ni}$  production. This is potentially possible by an abrupt change in the composition profile of the exploding WD as seen in hybrid WDs where a CO core is surrounded by an oxygen–neon (ONe) mantle. Such objects have recently been predicted by stellar evolution models (Denissenkov et al. 2013; Chen et al. 2014). Denissenkov et al. (2015) have shown that a thermonuclear runaway in accreting hybrid CONe WDs is possible when they approach  $M_{\text{Ch}}$ . Since hybrid CONe WDs originate from relatively massive zero-age main sequence (ZAMS) stars (Chen et al. 2014), such a scenario could also explain the short delay times of SNe Iax (Meng & Podsiadlowski 2014).

Here, we study a deflagration in such a near- $M_{\text{Ch}}$  hybrid CONe WD. The paper is organised as follows: in Section 2 we discuss the chosen progenitor model before we present our explosion simulation in Section 3. Synthetic observables for our model and comparison to observational data are presented in Section 4. In Section 5 we discuss our results and constraints on rates and delay times from binary population synthesis calculations before presenting our conclusion in Section 6.

## 2 PROGENITOR MODEL

In the single-degenerate progenitor scenario for SNe Ia, a CO WD is supposed to accrete H-rich material from a binary companion until it approaches  $M_{\text{Ch}}$  and a thermonuclear runaway occurs (e.g.

Hillebrandt & Niemeyer 2000, for a review). CO WDs are formed when the cores of asymptotic giant branch (AGB) stars are exposed after they have expelled their envelopes. In classical single-star evolution models the maximum mass for the CO core of an AGB star is  $\sim 1.05 M_{\odot}$  (Chen et al. 2014). For more massive cores, C burning is ignited (super-AGB phase) and the entire core is converted to O and Ne, leading to the formation of an ONe WD once the star has lost its envelope. ONe WDs have been discarded as progenitor candidates for the single-degenerate progenitor scenario of SNe Ia. It has been argued that they should undergo a gravitational collapse and form a neutron star rather than a thermonuclear explosion when approaching  $M_{\text{Ch}}$  (Nomoto 1984, 1987; Nomoto & Kondo 1991).

Recently, Denissenkov et al. (2013) and Chen et al. (2014) have shown that convective boundary mixing during the super-AGB phase can prevent off-centre ignited C burning from reaching the centre of the star, thus leaving a hybrid CONe WD with a C-rich core at the end of the super-AGB phase. In contrast to an ONe WD, such a hybrid WD with a C-rich core is likely to be able to trigger a thermonuclear explosion when approaching  $M_{\text{Ch}}$ . ONe-rich WDs containing a small fraction of unburnt C have been predicted by stellar evolution models previously (Siess 2006), and have been mentioned in the literature as possible progenitors of thermonuclear explosions (Garcia-Berro et al. 1997).

Denissenkov et al. (2015) have simulated the mass accretion onto hybrid CONe WDs to investigate their potential as SN Ia progenitors in the single-degenerate scenario. They find that a thermonuclear runaway in accreting hybrid CONe WDs is possible depending on the mass of the parent star and accretion history. The exact thermal and chemical structure of the hybrid WD at the time of explosion, however, is uncertain and can only be determined from 3D reactive-convective hydro simulations. In particular, a series of convective Urca shell flashes can either limit the mass of the convective C core or completely suppress convective mixing (Denissenkov et al. 2015).

Here, we investigate how a deflagration will incinerate a hybrid CONe WD that undergoes a thermonuclear runaway when approaching  $M_{\text{Ch}}$  and calculate synthetic observables to compare the optical display of such an explosion to observed SNe Ia(x). For this purpose we neglect the uncertainties regarding the exact structure of the progenitor and follow a simplified approach to model the hybrid CONe WD. Motivated by the model of Denissenkov et al. (2013), we choose the initial WD (central density  $\rho_c = 2.9 \times 10^9 \text{ g cm}^{-3}$  and isothermal temperature structure with  $T = 5 \times 10^5 \text{ K}$ ) to have a C-rich core of  $0.2 M_{\odot}$  ( $X(\text{C}) = 0.5$ ,  $X(\text{O}) = 0.5$ ), surrounded by an ONe layer ( $X(\text{C}) = 0.03$ ,  $X(\text{O}) = 0.5$ ,  $X(\text{Ne}) = 0.47$ ) up to  $1.1 M_{\odot}$ . On top of this, we place a layer of accreted material with  $X(\text{C}) = 0.5$ ,  $X(\text{O}) = 0.5$  which extends up to  $1.4 M_{\odot}$ .

## 3 EXPLOSION SIMULATION

To simulate the explosion phase we use our 3D hydro code LEAFS (based on the implementation by Reinecke et al. 2002). LEAFS solves the reactive Euler equations and models the propagation of deflagrations using a levelset scheme (Reinecke et al. 1999; Osher & Sethian 1988; Smiljanovski et al. 1997) and sub-grid scale turbulence model (Schmidt et al. 2006a,b) to account for flame acceleration by buoyancy- and shear-instability induced turbulent fluid flows. Self-gravity is dealt with by a monopole gravity solver and an equation of state appropriate for WD matter is used. To follow the evolution of the explosion ejecta to the phase of homologous ex-

pansion, we use the expanding grid technique described by Röpke (2005) and Röpke et al. (2006). For more information on the hydrodynamics code and details concerning the burning treatment see Fink et al. (2014).

In our progenitor WD as described in Section 2 we ignite a deflagration near the centre using the same asymmetric 5-kernel ignition configuration as in the N5def model of Kromer et al. (2013) and Fink et al. (2014). This model of the deflagration of a near- $M_{\text{Ch}}$  CO WD produces observables in good agreement with the Type Iax SN 2005hk (Kromer et al. 2013). Here, we follow the flame propagation in our hybrid CONe WD and the subsequent hydrodynamical evolution of the ejecta up to the phase of homologous expansion (see Figure 1).

After the burning starts from the 5 ignition kernels, the flames soon merge and a one-sided deflagration plume develops within the C-rich core. In the ONe layer above  $0.2 M_{\odot}$ , it is assumed that the C deflagration flame cannot propagate because of the small C fraction ( $X(\text{C}) = 0.03$ ). Thus, burning is switched off in the region initially consisting of mainly ONe matter and further out. Burning ceases at  $\sim 1.5$  s past explosion. The hot ashes rise to the surface and wrap around the unburnt parts of the progenitor WD. Due to the small nuclear energy released in the burning ( $E_{\text{nuc}} = 1.0 \times 10^{50}$  erg), only  $0.014 M_{\odot}$  of material is ejected while a massive bound remnant of  $1.39 M_{\odot}$  is left behind (the mass of the bound remnant and ejecta are determined as described by Kromer et al. 2013). We stop the simulation at 100 s after ignition. At that time the ejecta are in homologous expansion with an asymptotic kinetic energy of  $E_{\text{kin}} = 1.8 \times 10^{48}$  erg.

In a postprocessing calculation with a 384-isotope nuclear network (Travaglio et al. 2004) we determine the detailed chemical composition of the ejecta. To this end, about  $10^6$  Lagrangian tracer particles are passively advected in the hydrodynamic explosion simulation and thermodynamic trajectories are recorded for each tracer particle. The tracers are placed in the WD with variable masses according to the prescription by Seitenzahl et al. (2010). The initial composition of the tracer particles is drawn from the abundance profile of our progenitor WD.

Within the ejecta, we find  $6.41 \times 10^{-3} M_{\odot}$  of iron-group elements (IGEs), of which  $3.40 \times 10^{-3} M_{\odot}$  are  $^{56}\text{Ni}$ . The most abundant other species are O ( $3.49 \times 10^{-3} M_{\odot}$ ), C ( $2.73 \times 10^{-3} M_{\odot}$ ), Si ( $8.02 \times 10^{-4} M_{\odot}$ ) and S ( $3.56 \times 10^{-4} M_{\odot}$ ). The detailed composition of the ejecta is given in Tables 1 and 2.

Using an SPH-like algorithm (Kromer et al. 2010) we map the final composition of the unbound tracer particles to a  $200^3$  Cartesian grid to determine the abundance structure of the ejecta (see Figure 2). Our model shows significant deviations from spherical symmetry which is a consequence of the turbulent burning and the one-sided propagation of the thermonuclear flame within the progenitor WD.

For the bound remnant, which is not resolved in the hydrodynamics calculations, our nucleosynthesis post-processing is not reliable, since the tracers do not record accurate thermodynamic trajectories. Thus, we can only give approximate yields from the simplified description of nuclear reactions implemented in our hydro scheme. From this we find  $1.33 M_{\odot}$  unburnt material,  $3.3 \times 10^{-3} M_{\odot}$  intermediate-mass elements and  $5.3 \times 10^{-2} M_{\odot}$  IGEs, of which  $2.0 \times 10^{-2} M_{\odot}$  are  $^{56}\text{Ni}$ .

**Table 1.** Asymptotic chemical yields in the ejecta of our model.

	$M_{\odot}$		$M_{\odot}$
Total	$1.40 \times 10^{-2}$	Cl	$1.00 \times 10^{-6}$
He	$3.58 \times 10^{-7}$	Ar	$6.29 \times 10^{-5}$
Li	$3.90 \times 10^{-13}$	K	$6.98 \times 10^{-7}$
Be	$4.58 \times 10^{-13}$	Ca	$4.74 \times 10^{-5}$
B	$1.83 \times 10^{-11}$	Sc	$3.24 \times 10^{-9}$
C	$2.73 \times 10^{-3}$	Ti	$1.68 \times 10^{-6}$
N	$1.79 \times 10^{-7}$	V	$9.35 \times 10^{-7}$
O	$3.49 \times 10^{-3}$	Cr	$8.71 \times 10^{-5}$
F	$2.58 \times 10^{-9}$	Mn	$1.57 \times 10^{-4}$
Ne	$3.88 \times 10^{-4}$	Fe	$5.28 \times 10^{-3}$
Na	$1.75 \times 10^{-6}$	Co	$9.05 \times 10^{-6}$
Mg	$7.60 \times 10^{-5}$	Ni	$8.76 \times 10^{-4}$
Al	$3.78 \times 10^{-6}$	Cu	$5.74 \times 10^{-8}$
Si	$8.02 \times 10^{-4}$	Zn	$6.15 \times 10^{-8}$
P	$1.95 \times 10^{-6}$	Ga	$1.20 \times 10^{-9}$
S	$3.56 \times 10^{-4}$	Ge	$1.63 \times 10^{-9}$

**Table 2.** Yields of radioactive isotopes in the model ejecta at  $t = 100$  s.

	$M_{\odot}$		$M_{\odot}$
$^{56}\text{Ni}$	$3.40 \times 10^{-3}$	$^{59}\text{Fe}$	$8.15 \times 10^{-8}$
$^{57}\text{Ni}$	$1.29 \times 10^{-4}$	$^{52}\text{Mn}$	$4.95 \times 10^{-8}$
$^{55}\text{Co}$	$1.18 \times 10^{-4}$	$^{41}\text{Ca}$	$4.16 \times 10^{-8}$
$^{52}\text{Fe}$	$4.36 \times 10^{-5}$	$^{44}\text{Ti}$	$3.95 \times 10^{-8}$
$^{55}\text{Fe}$	$3.62 \times 10^{-5}$	$^{60}\text{Co}$	$3.02 \times 10^{-8}$
$^{57}\text{Co}$	$1.82 \times 10^{-5}$	$^{63}\text{Ni}$	$1.79 \times 10^{-8}$
$^{53}\text{Fe}$	$7.84 \times 10^{-6}$	$^{26}\text{Al}$	$1.34 \times 10^{-8}$
$^{59}\text{Ni}$	$7.56 \times 10^{-6}$	$^{35}\text{S}$	$2.73 \times 10^{-9}$
$^{53}\text{Mn}$	$3.96 \times 10^{-6}$	$^{65}\text{Zn}$	$2.42 \times 10^{-9}$
$^{56}\text{Co}$	$2.21 \times 10^{-6}$	$^{49}\text{V}$	$2.33 \times 10^{-9}$
$^{48}\text{Cr}$	$1.17 \times 10^{-6}$	$^{39}\text{Ar}$	$2.22 \times 10^{-9}$
$^{51}\text{Mn}$	$6.28 \times 10^{-7}$	$^{32}\text{P}$	$2.12 \times 10^{-9}$
$^{37}\text{Ar}$	$1.58 \times 10^{-7}$	$^{36}\text{Cl}$	$2.00 \times 10^{-9}$
$^{60}\text{Fe}$	$1.48 \times 10^{-7}$	$^{33}\text{P}$	$1.60 \times 10^{-9}$
$^{62}\text{Zn}$	$1.33 \times 10^{-7}$	$^{48}\text{V}$	$1.00 \times 10^{-9}$
$^{58}\text{Co}$	$1.21 \times 10^{-7}$	$^{40}\text{K}$	$6.25 \times 10^{-10}$
$^{54}\text{Mn}$	$1.12 \times 10^{-7}$	$^{22}\text{Na}$	$3.32 \times 10^{-10}$
$^{49}\text{Cr}$	$1.11 \times 10^{-7}$	$^{32}\text{Si}$	$2.81 \times 10^{-10}$
$^{14}\text{C}$	$1.07 \times 10^{-7}$	$^{68}\text{Ge}$	$7.98 \times 10^{-11}$
$^{51}\text{Cr}$	$9.11 \times 10^{-8}$	$^{65}\text{Ga}$	$1.43 \times 10^{-11}$

## 4 COMPARISON WITH OBSERVATIONS

Using our 3D Monte Carlo radiative transfer code ARTIS (Kromer & Sim 2009; Sim 2007) we calculate synthetic observables for the ejecta. To this end we re-map the abundance and density structure as obtained from the explosion simulation to a  $50^3$  Cartesian grid. On this grid we follow the propagation of  $1.2 \times 10^8$  Monte Carlo quanta for 136 logarithmic time steps from 0.3 to 35 d past explosion. Escaping Monte Carlo packets are binned in time and on a logarithmic wavelength grid spanning 10,000 bins from 600 to 30,000 Å to obtain a spectral time sequence. For our simulation we use the atomic data set as described by Gall et al. (2012). Local thermodynamic equilibrium is assumed for  $t < 0.42$  d and a grey approximation is used in optically thick cells (cf. Kromer & Sim 2009) to speed up the calculations.

Synthetic broad-band light curves of our model are shown in Figure 3. To examine the effects of asymmetries in the explosion ejecta (cf. Figure 2), we extract light curves along 100

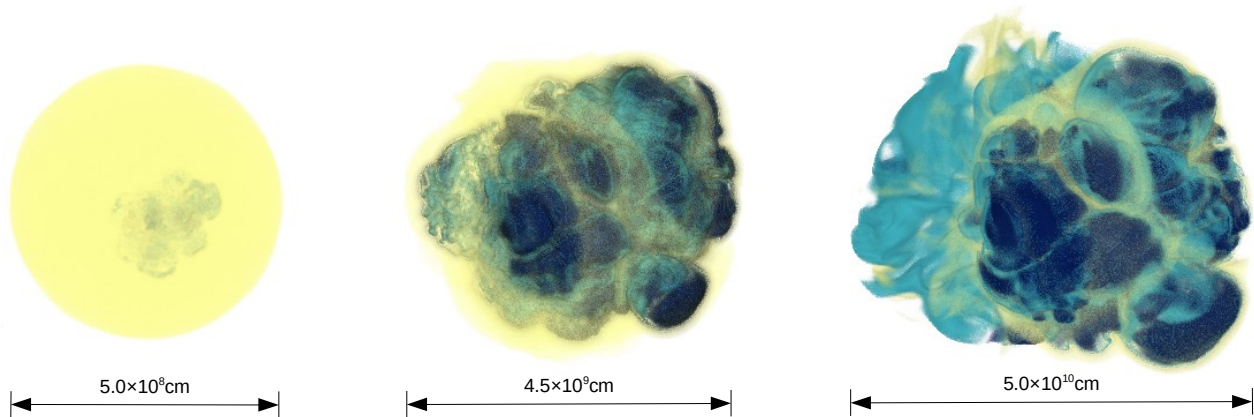


**Figure 1.** Hydrodynamical evolution of our model at 0.85, 2.5 and 10 s after explosion (from left to right). We show a volume rendering of the mean atomic number where yellow corresponds to unburnt material, and cyan and dark blue to ejecta rich in intermediate-mass or iron-group elements, respectively.

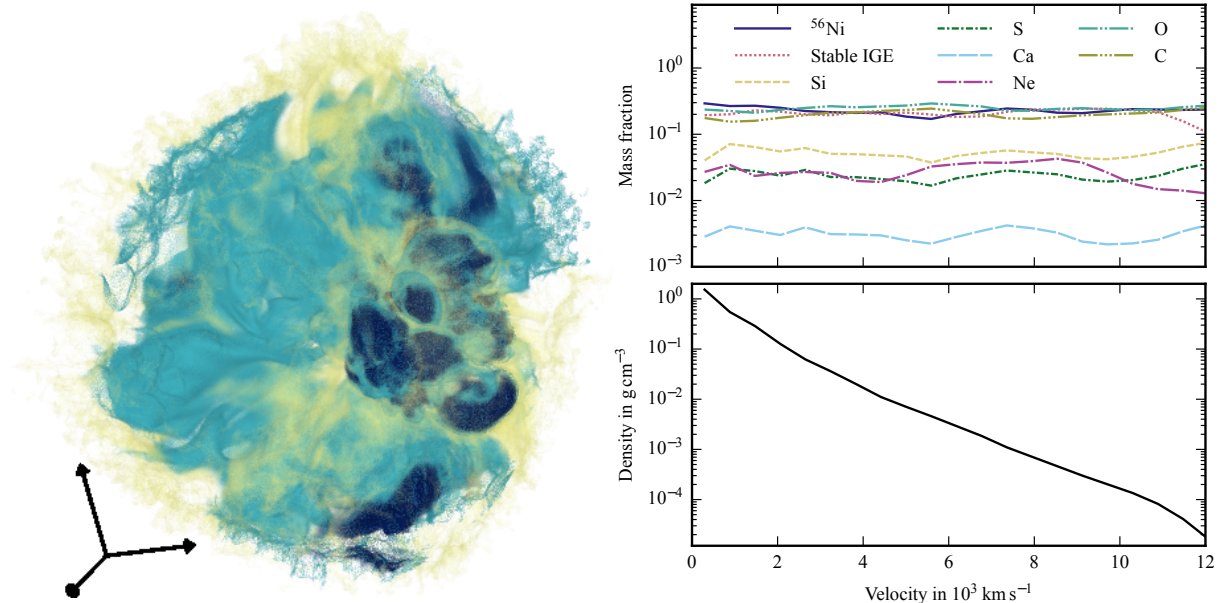


**Figure 2.** Final ejecta structure at 100 s. The left-hand panel shows a 3D volume rendering of the mean atomic number as in Figure 1 (the triad corresponds to a length of  $5 \times 10^{10}$  cm). The right-hand panel shows angle-averaged density and mass fractions of selected species as a function of expansion velocity.

different viewing angles sampling the full solid angle. The peak magnitudes of our model span a range from  $-13.2$  to  $-14.6$  and  $-14.2$  to  $-14.8$  in  $B$  and  $V$  band, respectively. These are significantly fainter than normal SNe Ia or proto-typical SNe Iax like SN 2002cx or SN 2005hk. Our peak magnitudes are, however, in good agreement with those of the faint Type Iax SN 2008ha ( $M_{\max}(B) = -13.74$  mag,  $M_{\max}(V) = -14.21$  mag; Foley et al. 2009). We also find reasonable agreement for the maximum-light colours along selected lines-of-sight.

However, our model light curves evolve significantly faster than SN 2008ha. This becomes obvious comparing the rise times of the model ( $t_{\max}(B) = 2.9 \dots 4.6$  d depending on the viewing angle) and SN 2008ha ( $\sim 10$  d; Foley et al. 2009), and also the decline of the redder bands at epochs later than  $\sim 10$  d past  $B$ -band maximum. The fast evolution of our model is a consequence of the extremely low ejecta mass of  $0.014 M_{\odot}$ , which is significantly smaller than the ejecta mass derived for SN 2008ha. Using analyt-

ical light curve models Foley et al. (2009) inferred an ejecta mass of  $M_{\text{ej}} = 0.15 M_{\odot}$  based on a first set of post-maximum observations. Including a pre-maximum spectrum to the analysis Foley et al. (2010) revised this estimate to  $M_{\text{ej}} = 0.30 M_{\odot}$  (Valenti et al. 2009 obtain an ejecta mass in the range 0.1 to  $0.5 M_{\odot}$ ).

As a consequence of the relatively strong asymmetry of the model ejecta, our light curves show stronger sensitivity to different viewing angles than those of the N5def model (Kromer et al. 2013). At peak the  $U$ -,  $B$ - and  $V$ -band magnitudes show a scatter of 2.3, 1.4 and 0.6 mag, respectively (Figure 3). Given the small sample size of faint SNe Iax and the large intrinsic diversity in the few systems known, this viewing angle sensitivity cannot be used to rule out the model.

Selected snapshots of the synthetic spectral time series resulting from our simulations are shown in Figure 4 and compared to observed spectra of SN 2008ha at corresponding epochs. At  $-1.2$  d (with respect to  $B$ -band maximum) our model agrees fairly well

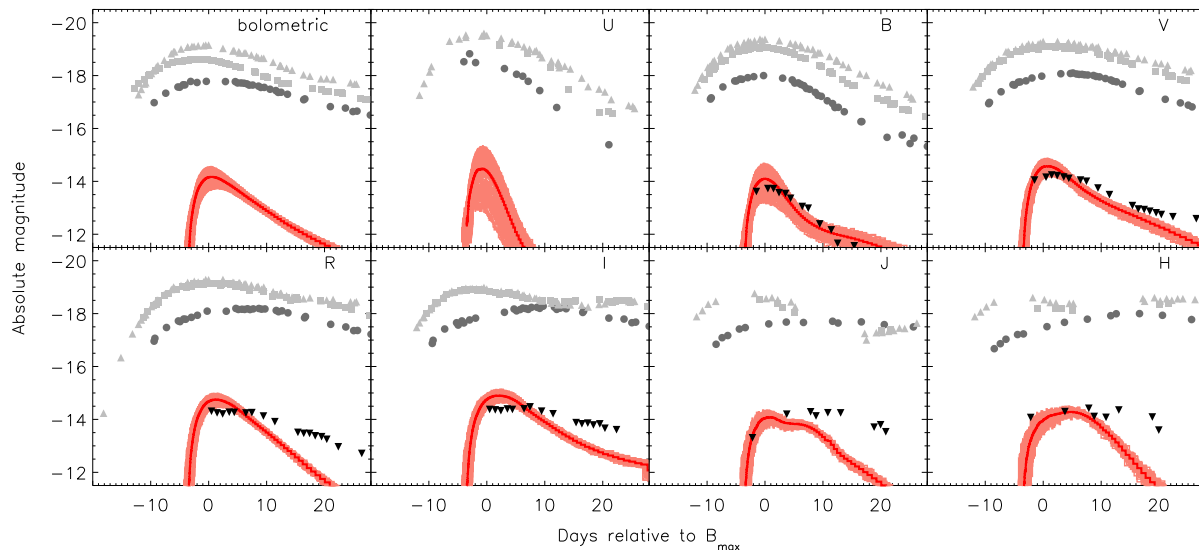


**Figure 3.** Synthetic light curves of our model for different filter bands as indicated in the panels. We show light curves from 100 different viewing angles (light red) sampling the full range of solid angle and the angle average (dark red). For comparison we show observational data for the normal SNe Ia 2004eo, 2005cf (grey squares and triangles, respectively), SN 2005hk (a proto-typical SN Iax, dark grey circles) and SN 2008ha (black upside-down triangles). The latter marks the faint end of the current sample of SNe Iax.

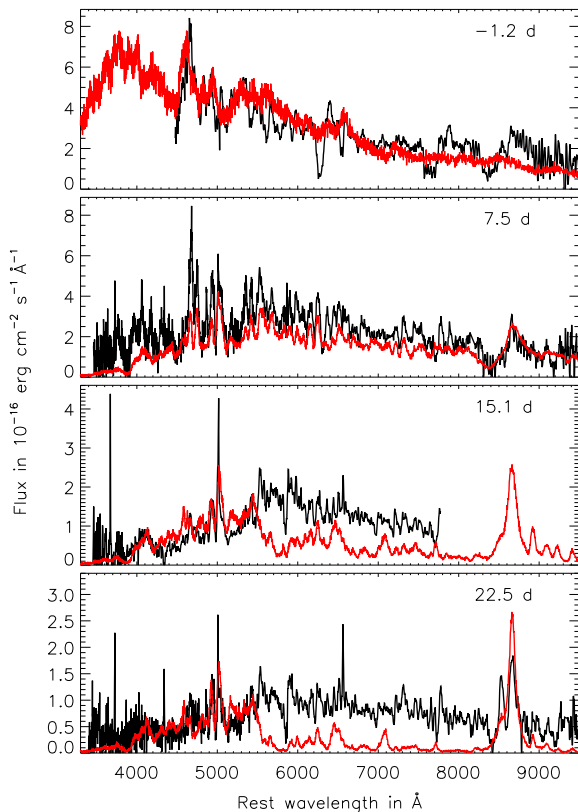


**Figure 4.** Angle-averaged synthetic spectra (in red) of our model at different epochs (times with respect to  $B$ -band maximum are indicated by the labels in the panels). For comparison, observed spectra of SN 2008ha (Foley et al. 2009, 2010; Valenti et al. 2009) are shown (the flux calibration has been checked against the photometry and adjusted if necessary). The observed spectra have been de-reddened and de-redshifted.

with the spectral energy distribution of SN 2008ha. However, the model fails to reproduce some of the narrow line features present in SN 2008ha, e.g. the features at  $6300 \text{ \AA}$ ,  $7600 \text{ \AA}$ , and  $8400 \text{ \AA}$  that have previously been identified with Si II, O I and Ca II, respectively (Foley et al. 2010). This could indicate a lack of intermediate-mass elements in the outer layers of the model ejecta.

Another explanation for the lack of narrow features in our model could be too large ejecta velocities. The model spectra are dominated by fluorescent emission in a plethora of atomic lines of IGEs, which are present throughout the ejecta in our model (see Figure 2). As long as the emission originates from the outer layers (where the expansion velocity is large) the emission lines are blended giving rise to a smooth pseudo continuum. With time the ejecta expand further, the outer layers become increasingly optically thin and deeper layers at lower velocities start to dominate the emission. Then individual lines de-blend and narrow features appear. A larger ejecta mass at similar energy release could reduce the ejecta velocities and thus lead to narrower line features.

A week after  $B$ -band maximum (7.5 d) the agreement between our model and SN 2008ha is fairly good. The model shows a forest of narrow line features similar to that observed in SN 2008ha though not every feature is reproduced perfectly. However, this cannot be expected from a model that is not tuned to fit the data. Even for normal SNe Ia, “first-principle” models do not perfectly reproduce the observed spectra (e.g. Sim et al. 2013), particularly if plotted in *absolute* fluxes as in Figure 4. In previous work the narrow line features were interpreted as P-Cygni absorption profiles (e.g. Foley et al. 2009). In our model most of the features can be attributed to fluorescent emission in lines of IGEs (see Figure 5).

At later epochs (15.1 d and 22.5 d) the agreement deteriorates. In particular, the rapid decrease of flux at wavelengths larger than  $5500 \text{ \AA}$  is not observed in SN 2008ha. This reflects the rapid decline in some of our broad-band light curves ( $R$  band and redder) discussed above and indicates that the model ejecta become optically thin too early, again pointing to a lack of ejecta mass in our model compared to SN 2008ha. At late epochs, however, some approximations on the plasma state, made in our radiative transfer code,

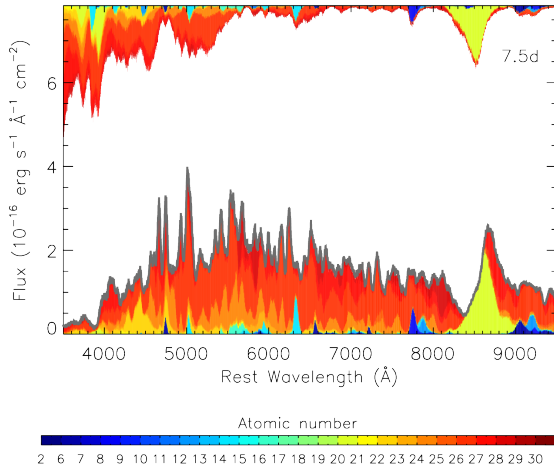


**Figure 5.** Angle-averaged synthetic spectrum of our model (grey) at 7.5 d past *B*-band maximum. The colour coding shows the chemical species responsible for both bound-bound emission and absorption of quanta in our Monte Carlo simulation. Below the synthetic spectrum, we colour code the fraction of escaping quanta in each wavelength bin that were last emitted by a particular chemical species (corresponding atomic numbers are illustrated in the colour bar). The coloured regions along the top of the plot indicate which elements were last responsible for removing quanta from a particular wavelength bin (either by absorption or scattering / fluorescence).

become less applicable (Kromer & Sim 2009). Indeed, we find that the agreement between synthetic observables and data deteriorates also for other model classes (e.g. Röpke et al. 2012). Thus, some of the differences at later epochs could also be due to systematics in the radiative transfer.

## 5 DISCUSSION

### 5.1 Ejecta mass

The lack of narrow line features around maximum light and the overly rapid light curve evolution of our model compared to SN 2008ha indicate that the ejecta mass of the model is too low. In contrast, the good agreement in peak luminosity suggests that the  $^{56}\text{Ni}$  yield in the model ejecta is close to that in SN 2008ha. Here, we have investigated a single realisation of a deflagration in a hybrid CONe WD for a particular progenitor structure and ignition setup. In reality both of these will show some diversity. The progenitor structure will depend on the accretion history and the final reactive-convective evolution of the WD core before the thermonuclear runaway, which will also determine the ignition setup. A thorough investigation of the parameter space is necessary to assess whether variations in these initial conditions can increase the ejecta mass while keeping the  $^{56}\text{Ni}$  mass in the ejecta similar, and thus lead to a better agreement with SN 2008ha. This requires a large number of explosion simulations and will be addressed in future work. Given the large uncertainty in the chemical and thermal structure of hybrid WDs (Denissenkov et al. 2015), here we focus on a simple model for an exploratory study.

### 5.2 Bound remnant

A key prediction of our model is a bound stellar remnant of  $\sim M_{\text{Ch}}$ . Recently, deep post-explosion *HST* images have revealed a

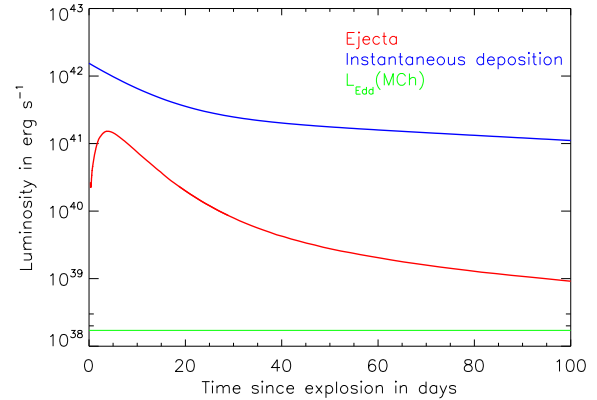


**Figure 6.** Bolometric light curve of the ejecta (red) and instantaneous energy deposition due to radioactive decay of  $^{56}\text{Ni}$  in the bound remnant (blue). For comparison the green line shows the Eddington luminosity of a  $M_{\text{Ch}}$  object. To obtain the bolometric light curve of the ejecta for the full time range, we have performed an additional low-resolution radiative transfer simulation from 2 to 120 d to extend our high-resolution simulation that stops at 35 d.

point source S1 at the site of the faint Type Ia SN 2008ha (Foley et al. 2014b). One possible interpretation of S1, proposed by Foley et al. (2014b), is that it could be an inflated stellar remnant of a failed deflagration. From our present simulations, which follow the evolution of the explosion ejecta on an expanding grid, we cannot resolve the structure and thermal state of the remnant. Thus we cannot compare our bound remnant to the observed properties of the point source. We note, however, that explosion energy deposited in the bound remnant could lead to an expanded envelope. Whether the expansion is sufficient to account for a radius of  $1500 R_{\odot}$  as derived for S1 (Foley et al. 2014b) remains to be seen. This question will be addressed in more detail with an adaptive grid code in future work.

Moreover, our simulations show that  $2.0 \times 10^{-2} M_{\odot}$  of  $^{56}\text{Ni}$  synthesized during the explosion stay in the bound remnant (see Section 3). This is  $\sim 6$  times larger than the  $^{56}\text{Ni}$  yield in the ejecta. Consequently, the instantaneous energy deposition by decaying  $^{56}\text{Ni}$  in the bound remnant is significantly larger than the bolometric luminosity of the ejecta derived from our radiative transfer simulations (see Figure 6). Again, our ignorance of the structure of the bound remnant makes it difficult to make a robust statement of how the decay energy will affect the observational display. If the  $^{56}\text{Ni}$  is located close to the surface of the remnant, it might drive further mass ejection and contribute significantly to the observed luminosity. In contrast, if most of the  $^{56}\text{Ni}$  is confined to the central regions of the stellar remnant, it might take a long time for the decay-deposited energy to diffuse to the surface of the remnant so that it becomes negligible for the observational display of the explosion.

Another interesting question concerns the long-term evolution of the bound remnant. Because the kinetic energy of the explosion is very low, the donor star is presumably not much affected by the impact of the ejecta (Liu et al. 2013). Thus, it is possible that accretion resumes once the remnant has relaxed into an equilibrium state. Since only a tiny fraction of the mass of the initial WD is ejected, it is likely that the bound remnant approaches the  $M_{\text{Ch}}$  limit again. Whether or not this may lead to subsequent deflagrations and thus a recurrent nature of some SNe Ia, depends on the chemical and thermal structure of the bound remnant. If the C frac-

tion in the bound remnant is low, an accretion-induced collapse and a neutron star might be the more probable outcome. As our current simulations are unable to resolve the bound remnant, we can not make a predictive statement about its final fate at this stage.

### 5.3 Burning in the ONe layer

In this work, we have assumed that deflagration burning ceases when the flame front reaches the ONe mantle of the hybrid WD. This assumption significantly reduces the energy release compared to deflagrations in CO WDs and is critical to obtain very low  $^{56}\text{Ni}$  masses as observed in faint SNe Iax. However, in principle, deflagrations are possible in ONe material as well (Timmes & Woosley 1992). Since the energy release from burning this fuel is lower, the flame slows down and its width increases more rapidly with lower fuel density than for deflagrations in CO material (Timmes & Woosley 1992). ONe deflagrations are therefore not expected to propagate at densities lower than  $\sim 10^9 \text{ g cm}^{-3}$ . In our model, the CO deflagration reaches the ONe layer when it has expanded to densities of  $\sim 1.2 \times 10^9 \text{ g cm}^{-3}$ , so some additional burning in the ONe material is possible. Detailed microscopic flame simulations are necessary, however, to assess our assumption that burning stalls shortly after the deflagration reaches the ONe layer.

### 5.4 Binary population synthesis - rates and constraints on delay times

It is important to assess the likelihood of such events from a theoretical standpoint: how frequent are the faint SNe Iax events? We evolved 300,000 binaries with  $Z=0.02$  from the ZAMS up to a Hubble time assuming a binary fraction of 70 percent using the population synthesis code STARTRACK (Belczynski et al. 2002, 2008). To obtain theoretical birthrates we first calculated the number of ONe WDs that approach  $M_{\text{Ch}}$  via stable Roche-lobe overflow from a stellar companion (see P-MDS model description in Ruiter et al. 2014). Typically, these systems are considered to lead to accretion-induced collapse and form neutron stars, but as discussed in Section 2, if these WDs contain some non-negligible fraction of unburnt C, they may instead lead to thermonuclear explosions.

The STARTRACK code currently does not account for the evolution of hybrid CONe WDs explicitly. However, it is reasonable to assume that if such hybrid WDs exist then the lower mass limit will occur near the boundary where, in our population models, a degenerate CO core is formed, and where C burning occurs non-explosively leading to the formation of a degenerate ONe core (the CO WD – ONe WD boundary; see Belczynski et al. (2008)). The upper limit for the hybrid core mass will lie somewhere within the range of masses that are canonically assumed to result in ‘pure’ ONe WDs.

Denissenkov et al. (2015) found that single stars with ZAMS masses between  $\sim 6.4$  and  $7.3 M_{\odot}$  produce CONe hybrid WDs. This same mass range cannot be extrapolated to interacting binary stars since a star that has lost or gained mass will follow a different course of evolution (and end up with a different core mass) than that of a single star with the same ZAMS mass. To estimate how many of our ONe WDs may contain some fraction of unburnt C in their cores, we checked the corresponding WD birth masses that arise from ZAMS single stars within this mass range in STARTRACK. The corresponding range is 1.193 to 1.325  $M_{\odot}$ . Here, we assume these (ONe-rich) WDs contain some fraction of unburnt C and thus are hybrid WDs. A small number of ONe WDs are found below this

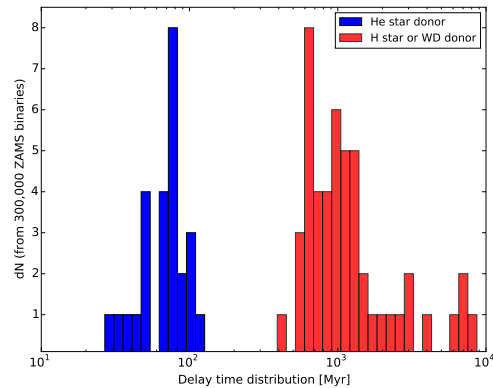


**Figure 7.** Delay time distribution of CONe WDs that approach  $M_{\text{Ch}}$  due to accretion from a binary star companion. Blue systems are those with helium-burning stars as donors while the red systems contain main-sequence, sub-giant, giant or WD donors. Numbers (y-axis) are not scaled to an absolute rate but rather represent the original numbers from our model. An estimate of absolute rates (over a Hubble time) is given in the text.

mass boundary in our model, and so we include these as potential hybrid cores as well. We assume all of these WDs undergo an off-centre deflagration once they approach  $M_{\text{Ch}}$ .

In terms of relative rates for different SN Ia progenitors, we find that over a Hubble time, hybrid CONe WDs that may produce faint Iax-like events are 1 percent of the rate of the entire CO-CO WD merger population. By comparison, they have about the same relative rate that we predict for the classic single-degenerate scenario at near solar metallicity, whereby a CO WD accretes toward  $M_{\text{Ch}}$  from a hydrogen-burning star (cf. table 1 of Marquardt et al., submitted). To put it in a more absolute context: Badenes & Maoz (2012) quote a SN Ia rate of  $1.1 \times 10^{-13} \text{ yr}^{-1} M_{\odot}^{-1}$  for Milky Way like galaxies. We find from our population synthesis model that the CO-CO WD merger rate (averaged over a Hubble time) is  $1.06 \times 10^{-13} \text{ yr}^{-1} M_{\odot}^{-1}$ , in other words: very close to the Sbc-like galaxy SN Ia rate (see also Li et al. 2011a). Taking this number at face value as the overall SN Ia rate, we find the rate of deflagrations in hybrid CONe WDs to be on the order of 1 percent of the SN Ia rate. This relative rate will increase, if one considers galaxies with active star formation rather than older stellar populations (like the Milky Way). Given the large uncertainties in the observed rate of SNe Iax (different authors give values between 5 and 30 percent of the overall rate of SNe Ia, Li et al. 2011b; Foley et al. 2013; White et al. 2015), our estimated rate seems in rough agreement with faint SNe Iax.

In Figure 7 we show the delay time distribution for the population of hybrid CONe WDs estimated from our population synthesis model. One third of our hybrid systems have delay times  $< 150$  Myr with the shortest delay time occurring at 30 Myr. All of our prompt systems below 150 Myr have helium-burning stars as donors (shown in blue). The range of delay times for these progenitors agrees with the results of Wang et al. (2014), who estimated the delay time range for CONe hybrid WDs that accrete toward  $M_{\text{Ch}}$  from helium stars to be 28 to 178 Myr. Our results are consistent with the fact that SNe Iax are found among young stellar populations; SN 2008ha is estimated to have a delay time of  $\lesssim 80$  Myr (Foley et al. 2014b). Nearly half of our hybrid systems, however, have hydrogen-burning donors, while 17 percent have He WD donors (all shown in red). All of these systems have longer

delay times (shortest one is 420 Myr). The main factor that determines whether a progenitor will have a very short delay time and a helium-burning star donor, or whether it will have a slightly longer delay time with a hydrogen-burning star (or WD) donor is the initial mass of the donor star. For the prompt systems, the ZAMS mass of the donor star ranges from 5–10  $M_{\odot}$  while for the rest, it ranges from 1–3  $M_{\odot}$ . Given our findings, it is unlikely that most progenitors of faint SN Iax events originate from systems with hydrogen-burning or WD donors, though our results strongly support the idea that faint SN Iax events arise from CONe WDs that accrete from helium burning stars.

## 6 CONCLUSION

Previous models of deflagrations in near- $M_{\text{Ch}}$  CO WDs had difficulties in explaining faint SNe Iax, since they produced significantly too large amounts of  $^{56}\text{Ni}$  (Fink et al. 2014). To reduce the  $^{56}\text{Ni}$  production, burning has to quench at an early stage. Deflagrations in hybrid CONe WDs, which have recently been predicted by stellar evolution models (Denissenkov et al. 2013; Chen et al. 2014), may lead to such a quenching when the burning front transitions from the WD’s CO-rich core to its ONe-rich mantle.

We have simulated an off-centre deflagration in a near- $M_{\text{Ch}}$  hybrid CONe WD. Assuming that the deflagration cannot propagate in the ONe layer, we find that only 0.014  $M_{\odot}$  of material is ejected while the remainder of the mass stays bound. The ejecta consist predominantly of IGEs, O, C, Si and S. Containing only  $3.4 \times 10^{-3} M_{\odot}$  of  $^{56}\text{Ni}$ , the ejecta will give rise to a faint transient.

Performing radiative transfer simulations for our model ejecta, we find peak absolute magnitudes in the range  $M_{\text{max}}^B = -13.2$  to  $-14.6$  mag depending on the viewing angle. This is in good agreement with the observed peak brightness of the faint Type Iax SN 2008ha ( $M_{\text{max}}^B = -13.7$  mag). Between peak and 10 d thereafter we also find reasonable agreement between the observed spectral shape of SN 2008ha and our model. This shows for the first time that deflagrations in near- $M_{\text{Ch}}$  hybrid CONe WDs can lead to faint transients with a display similar to faint SNe Iax.

However, our model still has some shortcomings. At epochs before maximum and later than 10 d past maximum the spectral evolution is too fast, probably indicating that the ejecta mass is too low. Since the exact thermal and chemical structure of  $M_{\text{Ch}}$  hybrid CONe WDs is not well constrained (Denissenkov et al. 2015), we used a simple model for the progenitor. Future work exploring a range of different initial conditions will show whether even better agreement with faint SNe Iax is possible from deflagrations in hybrid CONe WDs. More vigorous ignition setups, similar to those explored in CO WDs by Fink et al. (2014), or hybrid WDs with more massive CO cores might also be able to explain intermediate-luminosity SNe Iax like SN 2007qd (McClelland et al. 2010).

From binary population synthesis calculations we find that near- $M_{\text{Ch}}$  hybrid CONe WDs that may produce faint SNe Iax occur at a rate of 1 percent of the Galactic SN Ia rate. The delay times of these systems depend sensitively on the nature of the donor star. He-burning donors (delay times 30 to 150 Myr) are compatible with the estimated delay time of SN 2008ha (80 Myr, Foley et al. 2014a) and the observed preference for star-forming environment among SNe Iax (Lyman et al. 2013). H-burning and WD donors have somewhat longer delay times.

Finally, hydrodynamic simulations with adaptive grid codes will be needed to resolve the structure and thermal state of the

bound remnant predicted by our model. This will be crucial to assess the influence of the bound remnant on the observational display of the explosion and allow for a detailed comparison to the potential stellar remnant detected at the site of the faint SN 2008ha. Following the long-term evolution of the near- $M_{\text{Ch}}$  bound remnant and companion star will show whether subsequent mass-transfer episodes can lead to recurrent explosions or accretion-induced collapse.

## ACKNOWLEDGEMENTS

This work was supported by the Deutsche Forschungsgemeinschaft via the Transregional Collaborative Research Center TRR 33 ‘The Dark Universe’ and the Emmy Noether Program (RO 3676/1-1). Parts of this research were conducted by the Australian Research Council Centre of Excellence for All-sky Astrophysics (CAASTRO) through project number CE110001020 and by the the ARC Laureate Grant FL0992131.

AJR thanks A. Karakas and M. Childress for informative discussion. FKR is supported by the ARCHES prize of the German Ministry of Education and Research (BMBF). KSM acknowledges financial support from the DFG via the graduate school ‘Theoretical Astrophysics and Particle Physics’ at the University of Würzburg (GRK 1147). RP acknowledges support by the European Research Council under ERC-StG EXAGAL-308037 and by the Klaus Tschira Foundation. SAS acknowledges support from STFC grant ST/L000709/1. STO acknowledges financial support from Studienstiftung des deutschen Volkes. We also thank the DAAD/Go8 German-Australian exchange programme for travel support.

The authors gratefully acknowledge the Gauss Centre for Supercomputing (GCS) for providing computing time through the John von Neumann Institute for Computing (NIC) on the GCS share of the supercomputer JUQUEEN at Jülich Supercomputing Centre (JSC). GCS is the alliance of the three national supercomputing centres HLRS (Universität Stuttgart), JSC (Forschungszentrum Jülich), and LRZ (Bayerische Akademie der Wissenschaften), funded by the German Federal Ministry of Education and Research (BMBF) and the German State Ministries for Research of Baden-Württemberg (MWK), Bayern (StMWFK) and Nordrhein-Westfalen (MIWF).

## REFERENCES

- Badenes C., Maoz D., 2012, *ApJL*, 749, L11
- Belczynski K., Kalogera V., Bulik T., 2002, *ApJ*, 572, 407
- Belczynski K., Kalogera V., Rasio F. A., Taam R. E., Zezas A., Bulik T., Maccarone T. J., Ivanova N., 2008, *ApJS*, 174, 223
- Branch D., Baron E., Thomas R. C., Kasen D., Li W., Filippenko A. V., 2004, *PASP*, 116, 903
- Chen M. C., Herwig F., Denissenkov P. A., Paxton B., 2014, *MNRAS*, 440, 1274
- Chornock R., Filippenko A. V., Branch D., Foley R. J., Jha S., Li W., 2006, *PASP*, 118, 722
- Denissenkov P. A., Herwig F., Truran J. W., Paxton B., 2013, *ApJ*, 772, 37
- Denissenkov P. A., Truran J. W., Herwig F., Jones S., Paxton B., Nomoto K., Suzuki T., Toki H., 2015, *MNRAS*, 447, 2696
- Fink M. et al., 2014, *MNRAS*, 438, 1762



- Foley R. J., Brown P. J., Rest A., Challis P. J., Kirshner R. P., Wood-Vasey W. M., 2010, *ApJL*, 708, L61
- Foley R. J. et al., 2013, *ApJ*, 767, 57
- Foley R. J. et al., 2009, *AJ*, 138, 376
- Foley R. J. et al., 2014a, *MNRAS*, 443, 2887
- Foley R. J., McCully C., Jha S. W., Bildsten L., Fong W.-f., Narayan G., Rest A., Stritzinger M. D., 2014b, *ApJ*, 792, 29
- Gall E. E. E., Taubenberger S., Kromer M., Sim S. A., Benetti S., Blanc G., Elias-Rosa N., Hillebrandt W., 2012, *MNRAS*, 427, 994
- Garcia-Berro E., Ritossa C., Iben I. J., 1997, *ApJ*, 485, 765
- Hillebrandt W., Niemeyer J. C., 2000, *ARA&A*, 38, 191
- Jha S. et al., 2006, *AJ*, 131, 527
- Jordan, IV G. C., Perets H. B., Fisher R. T., van Rossum D. R., 2012, *ApJL*, 761, L23
- Kromer M. et al., 2013, *MNRAS*, 429, 2287
- Kromer M., Sim S. A., 2009, *MNRAS*, 398, 1809
- Kromer M., Sim S. A., Fink M., Röpke F. K., Seitenzahl I. R., Hillebrandt W., 2010, *ApJ*, 719, 1067
- Li W. et al., 2011a, *Nature*, 480, 348
- Li W. et al., 2003, *PASP*, 115, 453
- Li W. et al., 2011b, *MNRAS*, 412, 1441
- Liu Z.-W., Kromer M., Fink M., Pakmor R., Röpke F. K., Chen X. F., Wang B., Han Z. W., 2013, *ApJ*, 778, 121
- Lyman J. D., James P. A., Perets H. B., Anderson J. P., Gal-Yam A., Mazzali P., Percival S. M., 2013, *MNRAS*, 434, 527
- McClelland C. M. et al., 2010, *ApJ*, 720, 704
- McCully C. et al., 2014, *Nature*, 512, 54
- Meng X., Podsiadlowski P., 2014, *ApJL*, 789, L45
- Moriya T., Tominaga N., Tanaka M., Nomoto K., Sauer D. N., Mazzali P. A., Maeda K., Suzuki T., 2010, *ApJ*, 719, 1445
- Nomoto K., 1984, *ApJ*, 277, 791
- Nomoto K., 1987, *ApJ*, 322, 206
- Nomoto K., Kondo Y., 1991, *ApJL*, 367, L19
- Osher S., Sethian J. A., 1988, *Journal of Computational Physics*, 79, 12
- Phillips M. M. et al., 2007, *PASP*, 119, 360
- Reinecke M., Hillebrandt W., Niemeyer J. C., 2002, *A&A*, 386, 936
- Reinecke M., Hillebrandt W., Niemeyer J. C., Klein R., Gröbl A., 1999, *A&A*, 347, 724
- Röpke F. K., 2005, *A&A*, 432, 969
- Röpke F. K., Hillebrandt W., Niemeyer J. C., Woosley S. E., 2006, *A&A*, 448, 1
- Röpke F. K. et al., 2012, *ApJL*, 750, L19
- Ruiter A. J., Belczynski K., Sim S. A., Seitenzahl I. R., Kwiatkowski D., 2014, *MNRAS*, 440, L101
- Sahu D. K. et al., 2008, *ApJ*, 680, 580
- Schmidt W., Niemeyer J. C., Hillebrandt W., 2006a, *A&A*, 450, 265
- Schmidt W., Niemeyer J. C., Hillebrandt W., Röpke F. K., 2006b, *A&A*, 450, 283
- Seitenzahl I. R., Röpke F. K., Fink M., Pakmor R., 2010, *MNRAS*, 407, 2297
- Siess L., 2006, *A&A*, 448, 717
- Sim S. A., 2007, *MNRAS*, 375, 154
- Sim S. A. et al., 2013, *MNRAS*, 436, 333
- Smiljanovski V., Moser V., Klein R., 1997, *Combustion Theory Modelling*, 1, 183
- Stritzinger M. D. et al., 2014, *A&A*, 561, A146
- Stritzinger M. D. et al., 2015, *A&A*, 573, A2
- Timmes F. X., Woosley S. E., 1992, *ApJ*, 396, 649
- Travaglio C., Hillebrandt W., Reinecke M., Thielemann F.-K., 2004, *A&A*, 425, 1029
- Valenti S. et al., 2009, *Nature*, 459, 674
- Wang B., Meng X., Liu D.-D., Liu Z.-W., Han Z., 2014, *ApJL*, 794, L28
- White C. J. et al., 2015, *ApJ*, 799, 52